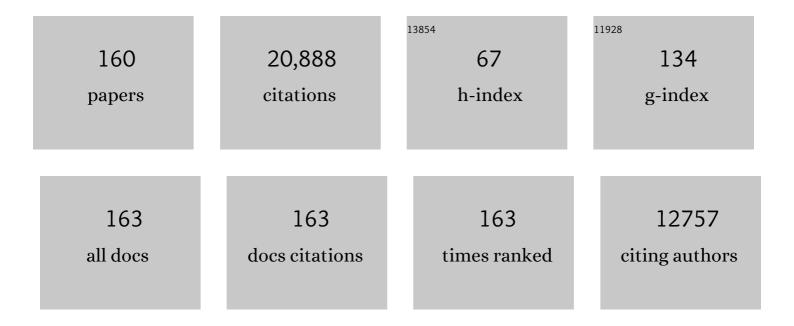
Pablo J Zarco-Tejada

List of Publications by Year in descending order

Source: https://exaly.com/author-pdf/7867196/publications.pdf Version: 2024-02-01



#	Article	IF	CITATIONS
1	Hyperspectral vegetation indices and novel algorithms for predicting green LAI of crop canopies: Modeling and validation in the context of precision agriculture. Remote Sensing of Environment, 2004, 90, 337-352.	4.6	1,819
2	Integrated narrow-band vegetation indices for prediction of crop chlorophyll content for application to precision agriculture. Remote Sensing of Environment, 2002, 81, 416-426.	4.6	1,379
3	PROSPECT+SAIL models: A review of use for vegetation characterization. Remote Sensing of Environment, 2009, 113, S56-S66.	4.6	1,178
4	Thermal and Narrowband Multispectral Remote Sensing for Vegetation Monitoring From an Unmanned Aerial Vehicle. IEEE Transactions on Geoscience and Remote Sensing, 2009, 47, 722-738.	2.7	972
5	Fluorescence, temperature and narrow-band indices acquired from a UAV platform for water stress detection using a micro-hyperspectral imager and a thermal camera. Remote Sensing of Environment, 2012, 117, 322-337.	4.6	747
6	Global and time-resolved monitoring of crop photosynthesis with chlorophyll fluorescence. Proceedings of the National Academy of Sciences of the United States of America, 2014, 111, E1327-33.	3.3	741
7	Assessing vineyard condition with hyperspectral indices: Leaf and canopy reflectance simulation in a row-structured discontinuous canopy. Remote Sensing of Environment, 2005, 99, 271-287.	4.6	589
8	Retrieval of foliar information about plant pigment systems from high resolution spectroscopy. Remote Sensing of Environment, 2009, 113, S67-S77.	4.6	576
9	Scaling-up and model inversion methods with narrowband optical indices for chlorophyll content estimation in closed forest canopies with hyperspectral data. IEEE Transactions on Geoscience and Remote Sensing, 2001, 39, 1491-1507.	2.7	529
10	Water content estimation in vegetation with MODIS reflectance data and model inversion methods. Remote Sensing of Environment, 2003, 85, 109-124.	4.6	450
11	Tree height quantification using very high resolution imagery acquired from an unmanned aerial vehicle (UAV) and automatic 3D photo-reconstruction methods. European Journal of Agronomy, 2014, 55, 89-99.	1.9	426
12	Quantitative Remote Sensing at Ultra-High Resolution with UAV Spectroscopy: A Review of Sensor Technology, Measurement Procedures, and Data Correction Workflows. Remote Sensing, 2018, 10, 1091.	1.8	375
13	Remote sensing of solar-induced chlorophyll fluorescence (SIF) in vegetation: 50†years of progress. Remote Sensing of Environment, 2019, 231, 111177.	4.6	372
14	High-resolution airborne hyperspectral and thermal imagery for early detection of Verticillium wilt of olive using fluorescence, temperature and narrow-band spectral indices. Remote Sensing of Environment, 2013, 139, 231-245.	4.6	354
15	Hyperspectral indices and model simulation for chlorophyll estimation in open-canopy tree crops. Remote Sensing of Environment, 2004, 90, 463-476.	4.6	332
16	Mapping canopy conductance and CWSI in olive orchards using high resolution thermal remote sensing imagery. Remote Sensing of Environment, 2009, 113, 2380-2388.	4.6	314
17	Steady-state chlorophyll a fluorescence detection from canopy derivative reflectance and double-peak red-edge effects. Remote Sensing of Environment, 2003, 84, 283-294.	4.6	297
18	High-Resolution Airborne UAV Imagery to Assess Olive Tree Crown Parameters Using 3D Photo Reconstruction: Application in Breeding Trials. Remote Sensing, 2015, 7, 4213-4232.	1.8	263

#	Article	IF	CITATIONS
19	Mapping crop water stress index in a â€~Pinot-noir' vineyard: comparing ground measurements with thermal remote sensing imagery from an unmanned aerial vehicle. Precision Agriculture, 2014, 15, 361-376.	3.1	261
20	Simple reflectance indices track heat and water stress-induced changes in steady-state chlorophyll fluorescence at the canopy scale. Remote Sensing of Environment, 2005, 97, 403-414.	4.6	259
21	Using high resolution UAV thermal imagery to assess the variability in the water status of five fruit tree species within a commercial orchard. Precision Agriculture, 2013, 14, 660-678.	3.1	255
22	Unmanned aerial platform-based multi-spectral imaging for field phenotyping of maize. Plant Methods, 2015, 11, 35.	1.9	248
23	Imaging chlorophyll fluorescence with an airborne narrow-band multispectral camera for vegetation stress detection. Remote Sensing of Environment, 2009, 113, 1262-1275.	4.6	242
24	A PRI-based water stress index combining structural and chlorophyll effects: Assessment using diurnal narrow-band airborne imagery and the CWSI thermal index. Remote Sensing of Environment, 2013, 138, 38-50.	4.6	237
25	Vegetation Stress Detection through Chlorophyll <i>a</i> + <i>b</i> Estimation and Fluorescence Effects on Hyperspectral Imagery. Journal of Environmental Quality, 2002, 31, 1433-1441.	1.0	229
26	Estimating leaf carotenoid content in vineyards using high resolution hyperspectral imagery acquired from an unmanned aerial vehicle (UAV). Agricultural and Forest Meteorology, 2013, 171-172, 281-294.	1.9	228
27	Assessing canopy PRI for water stress detection with diurnal airborne imagery. Remote Sensing of Environment, 2008, 112, 560-575.	4.6	224
28	Chlorophyll Fluorescence Effects on Vegetation Apparent Reflectance I. Leaf-Level Measurements and Model Simulation. Remote Sensing of Environment, 2000, 74, 582-595.	4.6	221
29	Previsual symptoms of Xylella fastidiosa infection revealed in spectral plant-trait alterations. Nature Plants, 2018, 4, 432-439.	4.7	212
30	Assessing structural effects on PRI for stress detection in conifer forests. Remote Sensing of Environment, 2011, 115, 2360-2375.	4.6	209
31	Temporal and Spatial Relationships between Within-Field Yield Variability in Cotton and High-Spatial Hyperspectral Remote Sensing Imagery. Agronomy Journal, 2005, 97, 641-653.	0.9	189
32	Detection of water stress in an olive orchard with thermal remote sensing imagery. Agricultural and Forest Meteorology, 2006, 136, 31-44.	1.9	186
33	Estimation of fuel moisture content by inversion of radiative transfer models to simulate equivalent water thickness and dry matter content: analysis at leaf and canopy level. IEEE Transactions on Geoscience and Remote Sensing, 2005, 43, 819-826.	2.7	175
34	Needle chlorophyll content estimation through model inversion using hyperspectral data from boreal conifer forest canopies. Remote Sensing of Environment, 2004, 89, 189-199.	4.6	174
35	Spatio-temporal patterns of chlorophyll fluorescence and physiological and structural indices acquired from hyperspectral imagery as compared with carbon fluxes measured with eddy covariance. Remote Sensing of Environment, 2013, 133, 102-115.	4.6	164
36	Early Detection and Quantification of Verticillium Wilt in Olive Using Hyperspectral and Thermal Imagery over Large Areas. Remote Sensing, 2015, 7, 5584-5610.	1.8	162

#	Article	IF	CITATIONS
37	Estimating vegetation water content with hyperspectral data for different canopy scenarios: Relationships between AVIRIS and MODIS indexes. Remote Sensing of Environment, 2006, 105, 354-366.	4.6	146
38	High-Throughput Estimation of Crop Traits: A Review of Ground and Aerial Phenotyping Platforms. IEEE Geoscience and Remote Sensing Magazine, 2021, 9, 200-231.	4.9	141
39	Field characterization of olive (Olea europaea L.) tree crown architecture using terrestrial laser scanning data. Agricultural and Forest Meteorology, 2011, 151, 204-214.	1.9	132
40	Relationships between net photosynthesis and steady-state chlorophyll fluorescence retrieved from airborne hyperspectral imagery. Remote Sensing of Environment, 2013, 136, 247-258.	4.6	130
41	Chlorophyll Fluorescence Effects on Vegetation Apparent Reflectance II. Laboratory and Airborne Canopy-Level Measurements with Hyperspectral Data. Remote Sensing of Environment, 2000, 74, 596-608.	4.6	125
42	Applicability and limitations of using the crop water stress index as an indicator of water deficits in citrus orchards. Agricultural and Forest Meteorology, 2014, 198-199, 94-104.	1.9	122
43	Estimating evaporation with thermal UAV data and two-source energy balance models. Hydrology and Earth System Sciences, 2016, 20, 697-713.	1.9	119
44	Carotenoid content estimation in a heterogeneous conifer forest using narrow-band indices and PROSPECT + DART simulations. Remote Sensing of Environment, 2012, 127, 298-315.	4.6	117
45	Modelling PRI for water stress detection using radiative transfer models. Remote Sensing of Environment, 2009, 113, 730-744.	4.6	116
46	Airborne Hyperspectral Images and Ground-Level Optical Sensors As Assessment Tools for Maize Nitrogen Fertilization. Remote Sensing, 2014, 6, 2940-2962.	1.8	114
47	Seasonal stability of chlorophyll fluorescence quantified from airborne hyperspectral imagery as an indicator of net photosynthesis in the context of precision agriculture. Remote Sensing of Environment, 2016, 179, 89-103.	4.6	112
48	Chlorophyll content estimation in an open-canopy conifer forest with Sentinel-2A and hyperspectral imagery in the context of forest decline. Remote Sensing of Environment, 2019, 223, 320-335.	4.6	112
49	Detecting water stress effects on fruit quality in orchards with time-series PRI airborne imagery. Remote Sensing of Environment, 2010, 114, 286-298.	4.6	107
50	Almond tree canopy temperature reveals intra-crown variability that is water stress-dependent. Agricultural and Forest Meteorology, 2012, 154-155, 156-165.	1.9	107
51	Monitoring water stress and fruit quality in an orange orchard under regulated deficit irrigation using narrow-band structural and physiological remote sensing indices. ISPRS Journal of Photogrammetry and Remote Sensing, 2012, 71, 47-61.	4.9	107
52	Land surface temperature derived from airborne hyperspectral scanner thermal infrared data. Remote Sensing of Environment, 2006, 102, 99-115.	4.6	104
53	Seasonal evolution of crop water stress index in grapevine varieties determined with high-resolution remote sensing thermal imagery. Irrigation Science, 2015, 33, 81-93.	1.3	102
54	Grape quality assessment in vineyards affected by iron deficiency chlorosis using narrow-band physiological remote sensing indices. Remote Sensing of Environment, 2010, 114, 1968-1986.	4.6	98

#	Article	lF	CITATIONS
55	A Novel Remote Sensing Approach for Prediction of Maize Yield Under Different Conditions of Nitrogen Fertilization. Frontiers in Plant Science, 2016, 7, 666.	1.7	98
56	Detection of water stress in orchard trees with a high-resolution spectrometer through chlorophyll fluorescence in-filling of the O/sub 2/-A band. IEEE Transactions on Geoscience and Remote Sensing, 2005, 43, 2860-2869.	2.7	94
57	Assessing the effects of forest health on sun-induced chlorophyll fluorescence using the FluorFLIGHT 3-D radiative transfer model to account for forest structure. Remote Sensing of Environment, 2017, 193, 165-179.	4.6	94
58	Automatic identification of agricultural terraces through object-oriented analysis of very high resolution DSMs and multispectral imagery obtained from an unmanned aerial vehicle. Journal of Environmental Management, 2014, 134, 117-126.	3.8	91
59	Early Detection and Quantification of Almond Red Leaf Blotch Using High-Resolution Hyperspectral and Thermal Imagery. Remote Sensing, 2016, 8, 276.	1.8	90
60	Land cover mapping at BOREAS using red edge spectral parameters from CASI imagery. Journal of Geophysical Research, 1999, 104, 27921-27933.	3.3	88
61	Vineyard irrigation scheduling based on airborne thermal imagery and water potential thresholds. Australian Journal of Grape and Wine Research, 2016, 22, 307-315.	1.0	88
62	Spaceborne Imaging Spectroscopy for Sustainable Agriculture: Contributions and Challenges. Surveys in Geophysics, 2019, 40, 515-551.	2.1	85
63	Airborne Thermal Imagery to Detect the Seasonal Evolution of Crop Water Status in Peach, Nectarine and Saturn Peach Orchards. Remote Sensing, 2016, 8, 39.	1.8	83
64	Airborne and ground level sensors for monitoring nitrogen status in a maize crop. Biosystems Engineering, 2017, 160, 124-133.	1.9	80
65	Remote sensing in BOREAS: Lessons learned. Remote Sensing of Environment, 2004, 89, 139-162.	4.6	76
66	Using High-Resolution Hyperspectral and Thermal Airborne Imagery to Assess Physiological Condition in the Context of Wheat Phenotyping. Remote Sensing, 2015, 7, 13586-13605.	1.8	75
67	Monitoring yield and fruit quality parameters in open-canopy tree crops under water stress. Implications for ASTER. Remote Sensing of Environment, 2007, 107, 455-470.	4.6	73
68	Understanding the temporal dimension of the red-edge spectral region for forest decline detection using high-resolution hyperspectral and Sentinel-2a imagery. ISPRS Journal of Photogrammetry and Remote Sensing, 2018, 137, 134-148.	4.9	71
69	Improved nitrogen retrievals with airborne-derived fluorescence and plant traits quantified from VNIR-SWIR hyperspectral imagery in the context of precision agriculture. International Journal of Applied Earth Observation and Geoinformation, 2018, 70, 105-117.	1.4	67
70	Mapping radiation interception in row-structured orchards using 3D simulation and high-resolution airborne imagery acquired from a UAV. Precision Agriculture, 2012, 13, 473-500.	3.1	62
71	Radiative transfer Vcmax estimation from hyperspectral imagery and SIF retrievals to assess photosynthetic performance in rainfed and irrigated plant phenotyping trials. Remote Sensing of Environment, 2019, 231, 111186.	4.6	61
72	High-resolution imagery acquired from an unmanned platform to estimate biophysical and geometrical parameters of olive trees under different irrigation regimes. PLoS ONE, 2019, 14, e0210804.	1.1	60

#	Article	IF	CITATIONS
73	Using radiometric surface temperature for surface energy flux estimation in Mediterranean drylands from a two-source perspective. Remote Sensing of Environment, 2013, 136, 234-246.	4.6	59
74	Evaluating the performance of xanthophyll, chlorophyll and structure-sensitive spectral indices to detect water stress in five fruit tree species. Precision Agriculture, 2018, 19, 178-193.	3.1	58
75	Early Diagnosis of Vegetation Health From High-Resolution Hyperspectral and Thermal Imagery: Lessons Learned From Empirical Relationships and Radiative Transfer Modelling. Current Forestry Reports, 2019, 5, 169-183.	3.4	58
76	Detection of downy mildew of opium poppy using high-resolution multi-spectral and thermal imagery acquired with an unmanned aerial vehicle. Precision Agriculture, 2014, 15, 639-661.	3.1	57
77	The normalized topographic method: an automated procedure for gully mapping using GIS. Earth Surface Processes and Landforms, 2014, 39, 2002-2015.	1.2	55
78	Improving the precision of irrigation in a pistachio farm using an unmanned airborne thermal system. Irrigation Science, 2015, 33, 43-52.	1.3	55
79	Detection of Xylella fastidiosa infection symptoms with airborne multispectral and thermal imagery: Assessing bandset reduction performance from hyperspectral analysis. ISPRS Journal of Photogrammetry and Remote Sensing, 2020, 162, 27-40.	4.9	55
80	Monitoring the incidence of Xylella fastidiosa infection in olive orchards using ground-based evaluations, airborne imaging spectroscopy and Sentinel-2 time series through 3-D radiative transfer modelling. Remote Sensing of Environment, 2020, 236, 111480.	4.6	49
81	Spatial Resolution Effects on Chlorophyll Fluorescence Retrieval in a Heterogeneous Canopy Using Hyperspectral Imagery and Radiative Transfer Simulation. IEEE Geoscience and Remote Sensing Letters, 2013, 10, 937-941.	1.4	48
82	Estimation of chlorophyll fluorescence under natural illumination from hyperspectral data. International Journal of Applied Earth Observation and Geoinformation, 2001, 3, 321-327.	1.4	45
83	High spatial resolution monitoring land surface energy, water and CO2 fluxes from an Unmanned Aerial System. Remote Sensing of Environment, 2019, 229, 14-31.	4.6	43
84	Unmixing-Based Fusion of Hyperspatial and Hyperspectral Airborne Imagery for Early Detection of Vegetation Stress. IEEE Journal of Selected Topics in Applied Earth Observations and Remote Sensing, 2014, 7, 2571-2582.	2.3	42
85	Multi-Temporal and Spectral Analysis of High-Resolution Hyperspectral Airborne Imagery for Precision Agriculture: Assessment of Wheat Grain Yield and Grain Protein Content. Remote Sensing, 2018, 10, 930.	1.8	41
86	Hotspots in the genomic architecture of field drought responses in wheat as breeding targets. Functional and Integrative Genomics, 2019, 19, 295-309.	1.4	40
87	Divergent abiotic spectral pathways unravel pathogen stress signals across species. Nature Communications, 2021, 12, 6088.	5.8	40
88	Advantages of retrieving pigment content [μg/cm2] versus concentration [%] from canopy reflectance. Remote Sensing of Environment, 2019, 230, 111195.	4.6	38
89	A new era in remote sensing of crops with unmanned robots. SPIE Newsroom, 2008, , .	0.1	37
90	FluorMODgui V3.0: A graphic user interface for the spectral simulation of leaf and canopy chlorophyll fluorescence. Computers and Geosciences, 2006, 32, 577-591.	2.0	36

#	Article	IF	CITATIONS
91	Discriminating irrigated and rainfed olive orchards with thermal ASTER imagery and DART 3D simulation. Agricultural and Forest Meteorology, 2009, 149, 962-975.	1.9	36
92	Soil Temperature Determines the Reaction of Olive Cultivars to Verticillium dahliae Pathotypes. PLoS ONE, 2014, 9, e110664.	1.1	34
93	A Novel Methodology to Estimate Single-Tree Biophysical Parameters from 3D Digital Imagery Compared to Aerial Laser Scanner Data. Remote Sensing, 2014, 6, 11627-11648.	1.8	34
94	Effects of Heterogeneity within Tree Crowns on Airborne-Quantified SIF and the CWSI as Indicators of Water Stress in the Context of Precision Agriculture. Remote Sensing, 2018, 10, 604.	1.8	32
95	Transpiration from canopy temperature: Implications for the assessment of crop yield in almond orchards. European Journal of Agronomy, 2019, 105, 78-85.	1.9	32
96	Modelling hyperspectral- and thermal-based plant traits for the early detection of Phytophthora-induced symptoms in oak decline. Remote Sensing of Environment, 2021, 263, 112570.	4.6	32
97	Model inversion for chlorophyll estimation in open canopies from hyperspectral imagery. International Journal of Remote Sensing, 2008, 29, 5093-5111.	1.3	30
98	Determining Biophysical Parameters for Olive Trees Using CASIâ€Airborne and Quickbird‣atellite Imagery. Agronomy Journal, 2011, 103, 644-654.	0.9	30
99	Modeling canopy water content for carbon estimates from MODIS data at land EOS validation sites. , 0, , .		29
100	Genetic dissection of agronomic and quality traits based on association mapping and genomic selection approaches in durum wheat grown in Southern Spain. PLoS ONE, 2019, 14, e0211718.	1.1	29
101	Discriminating Xylella fastidiosa from Verticillium dahliae infections in olive trees using thermal- and hyperspectral-based plant traits. ISPRS Journal of Photogrammetry and Remote Sensing, 2021, 179, 133-144.	4.9	29
102	Unmanned Aerial System multispectral mapping for low and variable solar irradiance conditions: Potential of tensor decomposition. ISPRS Journal of Photogrammetry and Remote Sensing, 2019, 155, 58-71.	4.9	28
103	Deriving Predictive Relationships of Carotenoid Content at the Canopy Level in a Conifer Forest Using Hyperspectral Imagery and Model Simulation. IEEE Transactions on Geoscience and Remote Sensing, 2014, 52, 5206-5217.	2.7	27
104	Impact of the spatial resolution on the energy balance components on an open-canopy olive orchard. International Journal of Applied Earth Observation and Geoinformation, 2019, 74, 88-102.	1.4	27
105	The Bioindicators of Forest Condition Project: A physiological, remote sensing approach. Forestry Chronicle, 2000, 76, 941-952.	0.5	26
106	Thermal remote sensing from Airborne Hyperspectral Scanner data in the framework of the SPARC and SEN2FLEX projects: an overview. Hydrology and Earth System Sciences, 2009, 13, 2031-2037.	1.9	25
107	Detection of Xylella fastidiosa in almond orchards by synergic use of an epidemic spread model and remotely sensed plant traits. Remote Sensing of Environment, 2021, 260, 112420.	4.6	24
108	Assessing the contribution of understory sun-induced chlorophyll fluorescence through 3-D radiative transfer modelling and field data. Remote Sensing of Environment, 2021, 253, 112195.	4.6	22

#	Article	IF	CITATIONS
109	Simultaneous assessment of nitrogen and water status in winter wheat using hyperspectral and thermal sensors. European Journal of Agronomy, 2021, 127, 126287.	1.9	21
110	Using hyperspectral plant traits linked to photosynthetic efficiency to assess N and P partition. ISPRS Journal of Photogrammetry and Remote Sensing, 2020, 169, 406-420.	4.9	19
111	Residual Effect and N Fertilizer Rate Detection by High-Resolution VNIR-SWIR Hyperspectral Imagery and Solar-Induced Chlorophyll Fluorescence in Wheat. IEEE Transactions on Geoscience and Remote Sensing, 2022, 60, 1-17.	2.7	18
112	Hyperspectral mapping of crop and soils for precision agriculture. , 2006, 6298, 84.		17
113	Monitoring biochemical limitations to photosynthesis in N and P-limited radiata pine using plant functional traits quantified from hyperspectral imagery. Remote Sensing of Environment, 2020, 248, 112003.	4.6	16
114	Spatio-Temporal Relationships between Optical Information and Carbon Fluxes in a Mediterranean Tree-Grass Ecosystem. Remote Sensing, 2017, 9, 608.	1.8	15
115	Evaluation of SIF retrievals from narrow-band and sub-nanometer airborne hyperspectral imagers flown in tandem: Modelling and validation in the context of plant phenotyping. Remote Sensing of Environment, 2022, 273, 112986.	4.6	15
116	Estimating Radiation Interception in Heterogeneous Orchards Using High Spatial Resolution Airborne Imagery. IEEE Geoscience and Remote Sensing Letters, 2014, 11, 579-583.	1.4	13
117	Breaking down barriers between remote sensing and plant pathology. Tropical Plant Pathology, 2019, 44, 398-400.	0.8	13
118	Evaluating the role of solar-induced fluorescence (SIF) and plant physiological traits for leaf nitrogen assessment in almond using airborne hyperspectral imagery. Remote Sensing of Environment, 2022, 279, 113141.	4.6	13
119	Relationships between Moderate Resolution Imaging Spectroradiometer water indexes and tower flux data in an old growth conifer forest. Journal of Applied Remote Sensing, 2007, 1, 013513.	0.6	12
120	Canopy optical indices from infinite reflectance and canopy reflectance models for forest condition monitoring: application to hyperspectral CASI data. , 0, , .		11
121	Estimating radiation interception in an olive orchard using physical models and multispectral airborne imagery. Israel Journal of Plant Sciences, 2012, 60, 107-121.	0.3	11
122	Reply to Magnani et al.: Linking large-scale chlorophyll fluorescence observations with cropland gross primary production. Proceedings of the National Academy of Sciences of the United States of America, 2014, 111, E2511.	3.3	11
123	Maximizing the relationship of yield to site-specific management zones with object-oriented segmentation of hyperspectral images. Precision Agriculture, 2018, 19, 348-364.	3.1	11
124	Empirical validation of the relationship between the crop water stress index and relative transpiration in almond trees. Agricultural and Forest Meteorology, 2020, 292-293, 108128.	1.9	11
125	A Heritage Science Workflow to Preserve and Narrate a Rural Archeological Landscape Using Virtual Reality: The Cerro del Castillo of Belmez and Its Surrounding Environment (Cordoba, Spain). Applied Sciences (Switzerland), 2020, 10, 8659.	1.3	11
126	Physical model inversion of the green spectral region to track assimilation rate in almond trees with an airborne nano-hyperspectral imager. Remote Sensing of Environment, 2021, 252, 112147.	4.6	11

Pablo J Zarco-Tejada

#	Article	IF	CITATIONS
127	Long-term effects of water stress on hyperspectral remote sensing indicators in young radiata pine. Forest Ecology and Management, 2021, 502, 119707.	1.4	11
128	Progress on the development of an integrated canopy fluorescence model. , 0, , .		9
129	PROSPECT+SAIL: 15 Years of Use for Land Surface Characterization. , 2006, , .		9
130	Normalization of the crop water stress index to assess the within-field spatial variability of water stress sensitivity. Precision Agriculture, 2021, 22, 964-983.	3.1	9
131	Assessing wine grape quality parameters using plant traits derived from physical model inversion of hyperspectral imagery. Agricultural and Forest Meteorology, 2021, 306, 108445.	1.9	9
132	Boreal forest mapping at the BOREAS study area using seasonal optical indices sensitive to plant pigment content. Canadian Journal of Remote Sensing, 2008, 34, S158-S171.	1.1	7
133	Retrieval of biophysical vegetation parameters using simultaneous inversion of high resolution remote sensing imagery constrained by a vegetation index. Precision Agriculture, 2013, 14, 541-557.	3.1	7
134	Retrieval of Quantitative and Qualitative Information about Plant Pigment Systems from High Resolution Spectroscopy. , 2006, , .		6
135	REMOTE SENSING OF THERMAL WATER STRESS INDICATORS IN PEACH. Acta Horticulturae, 2012, , 325-331.	0.1	5
136	Assessment of peach trees water status and leaf gas exchange using on-the-ground versus airborne-based thermal imagery. Agricultural Water Management, 2022, 267, 107628.	2.4	5
137	Chlorophyll content estimation of Boreal conifers using hyperspectral remote sensing. , 0, , .		4
138	Extracting tree crown properties from ground-based scanning laser data. , 2007, , .		3
139	ORCHARD WATER STRESS DETECTION USING HIGH-RESOLUTION IMAGERY. Acta Horticulturae, 2011, , 35-39.	0.1	3
140	Using Sentinel-2 Imagery to Track Changes Produced by Xylella Fastidiosa in Olive Trees. , 2018, , .		3
141	Assessment of Satellite Chlorophyll-Based Leaf Maximum Carboxylation Rate (Vcmax) Using Flux Observations at Crop and Grass Sites. IEEE Journal of Selected Topics in Applied Earth Observations and Remote Sensing, 2021, 14, 5352-5360.	2.3	3
142	Remote Sensing of Solar-Induced Chlorophyll Fluorescence from Vegetation Hyperspectral Reflectance and Radiative Transfer Simulation. , 2002, , 233-269.		3
143	Tree crown parameters assessment using 3D photo reconstruction as a tool for selection in olive breeding programs. Acta Horticulturae, 2017, , 1-4.	0.1	3
144	A tool for detecting crop water status using airborne high-resolution thermal imagery. , 2014, , .		3

#	Article	IF	CITATIONS
145	High resolution remote and proximal sensing to assess low and high yield areas in a wheat field. , 2015, , 191-198.		3
146	THE PHOTOCHEMICAL REFLECTANCE INDEX (PRI) AS A WATER STRESS INDICATOR IN PEACH ORCHARDS FROM REMOTE SENSING IMAGERY. Acta Horticulturae, 2012, , 363-369.	0.1	2
147	Using support vector machines to automatically extract open water signatures from POLDER multi-angle data over boreal regions. , 0, , .		1
148	Stress detection in orchards with hyperspectral remote sensing data. , 2006, 6359, 240.		1
149	Canopy water content estimates with AVIRIS imagery and MODIS reflectance products. , 2006, , .		1
150	Estimation of evapotranspiration on discontinuous crop canopies using high resolution thermal imagery. , 2007, , .		1
151	Assessment of the Spatial Varability of CWSI Within Almond Tree Crowns and its Effects on the Relationship with Stomatal Conductance. , 2018, , .		1
152	Using an unmanned platform and VIS-NIR cameras to determine biophysical and geometrical parameters of olive, grapevine and citrus canopies. Acta Horticulturae, 2021, , 345-352.	0.1	1
153	Comparing the Retrieval of Chlorophyll Fluorescence from Two Airborne Hyperspectral Imagers with Different Spectral Resolutions for Plant Phenotyping Studies. , 2021, , .		1
154	Minimization of shadow effects in forest canopies for chlorophyll content estimation using red edge optical indices through radiative transfer: implications for MERIS. , 0, , .		0
155	Detecting crop irrigation status in orchard canopies with airborne and ASTER thermal imagery. , 2007, , \cdot		0
156	Surface temperature in the context of FLuorescence EXplorer (FLEX) mission. , 2007, , .		0
157	RESPONSES OF NECTARINE TO REGULATED DEFICIT IRRIGATION AT THE FIELD SCALE. Acta Horticulturae, 2012, , 349-353.	0.1	Ο
158	Monitoring Forest Health with Sun-Induced Chlorophyll Fluorescence Observations and 3-D Radiative Transfer Modeling. , 2018, , .		0
159	38. Integrating vegetation vigour in a thermal sensitivity index for mapping the variability of orchard water stress. , 2021, , .		0
160	RESPONSE TO REGULATED DEFICIT IRRIGATION OF A NECTARINE ORCHARD IN SOUTHERN SPAIN. Acta Horticulturae, 2011, , 217-220.	0.1	0